Non-intrusive determination of the unsteady surface pressure and aerodynamic loads on a pitching airfoil

Mertens, C.; Sciacchitano, A.; van Oudheusden, B. W.; Sodja, J.

DOI
10.1088/1757-899X/1024/1/012051

Publication date
2021

Document Version
Final published version

Published in
IOP Conference Series: Materials Science and Engineering

Non-intrusive determination of the unsteady surface pressure and aerodynamic loads on a pitching airfoil

Non-intrusive determination of the unsteady surface pressure and aerodynamic loads on a pitching airfoil

C Mertens, A Sciacchitano, B W van Oudheusden and J Sodja
Faculty of Aerospace Engineering, Delft University of Technology
Kluyverweg 1, 2629HS Delft, The Netherlands

E-mail: C.Mertens@tudelft.nl

Abstract. The unsteady surface pressure distribution and aerodynamic loads on a pitching airfoil are determined non-intrusively using PIV measurements. An experimental test case is considered where the flow around the airfoil is mostly attached while the unsteady effects on the aerodynamic loads are significant. The surface pressure is calculated from the flow velocity measurements in the vicinity of the airfoil surface, that are obtained with a robotic PIV system, by using relations from unsteady potential flow and thin airfoil theory. The proposed approach is a robust and computationally efficient approach to obtain non-intrusive measurements of the unsteady surface pressure distribution and the aerodynamic loads, that are in good agreement with reference data from installed pressure transducer sensors.

1. Introduction

Unsteady fluid-structure interaction (FSI) experiments are necessary for generating reference data to validate computational models, for example in the design of novel aircraft configurations. An important parameter in the characterization of FSIs is the magnitude and distribution of the aerodynamic load. The use of installed pressure transducers for the measurement of the unsteady surface pressure and aerodynamic loads in these experiments is challenging, because the integration of the sensors in the experimental model is associated with significant costs, possibly intrudes the experimental measurements and it additionally suffers from a relatively low spatial resolution. An alternative approach is to infer the aerodynamic loads from flow field measurements that are obtained non-intrusively with particle image velocimetry (PIV). However, a straightforward and computationally efficient method to determine the surface pressure on moving airfoils in unsteady flow conditions based on non-intrusive PIV measurements, for instance in large-scale aeroelasticity experiments, is still missing.

A popular method for the PIV-based surface pressure determination is the numerical solution of the Poisson equation for the pressure in incompressible flow, after the pressure gradient throughout the flow field has been calculated from the flow velocity measurements using the momentum equation in its differential form [1]. The numerical solution of the pressure Poisson equation involves Dirichlet boundary conditions placed sufficiently far away from the object, where Bernoulli's equation is used to calculate the pressure in regions where the flow is irrotational [2]. It was shown by Villegas and Diez [3] that the use of Bernoulli's equation in a quasi-steady sense is unsuited to determine the loads on unsteady airfoils with this approach. A correction to the Bernoulli equation has been proposed based for a purely advective unsteadiness [4,5], but this is not appropriate for a pitching airfoil in attached flow conditions.

An alternative approach to determine the surface pressure is to directly apply an analytical relation between the pressure and the measured flow velocity in the vicinity of the airfoil, such as Bernoulli's equation for steady potential flow or the isentropic relation in the case of compressible flow [6,7]. This approach is computationally efficient, but a consideration of the limitations of the analytical relations, that do not account e.g. for turbulence or boundary layer effects, is necessary in its implementation [8]. In this study, the unsteady surface pressure and aerodynamic loads on a pitching airfoil are determined from flow velocity measurements using a combination of relations from unsteady potential flow and thin airfoil theory.

2. Experimental configuration

2.1. Wind tunnel setup

An experiment was conducted in the Open Jet Facility (OJF) at Delft University of Technology. The OJF is an open test section, closed return wind tunnel with an octagonal outlet ($2.85 \times 2.85\,\mathrm{m}^2$), which was operated at a freestream velocity of $U_\infty = 5.6\,\mathrm{m/s}$ during the experiment, corresponding to Reynolds number $Re = 150\,000$ based on the chord length $c = 0.4\,\mathrm{m}$. A photo of the wind tunnel setup with an indication of the relevant components is shown in figure 1.

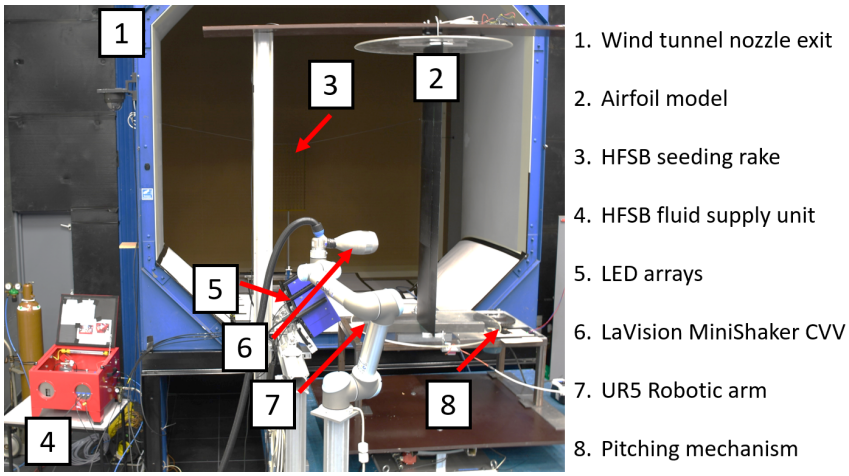

Figure 1. Photo of the experimental setup, looking upstream

The experimental model is a rigid rectangular wing section (span width $s = 1.45\,\mathrm{m}$) with a NACA 0018 airfoil section that is equipped with 24 Honeywell HSCS-RRN-1.6MD-SA5 differential pressure transducers installed inside the airfoil model to measure the pressure difference between the model top and bottom surface. Pressure transducer measurements are acquired over 45 pitching cycles at a sampling rate of $f_s = 32\,\mathrm{Hz}$ to obtain reference data for the PIV-based pressure determination. To prevent laminar boundary layer separation near the airfoil leading edge, a zig-zag turbulator strip (thickness 2 mm, width 12 mm, pitch 60°) is installed on both sides of the model at $x/c = 0.1$. For the experiment, the investigated airfoil model is mounted vertically in the wind tunnel test section and equipped with two circular end plates, where the top plate is attached to a support frame and the bottom plate is mounted on a steel frame that also holds the pitching mechanism. The pitching mechanism consists of a flywheel and a linkage rod to convert the rotation of a frequency-controlled AC motor to angle of attack oscillations $\alpha(t)$ of the model around the pitch axis, which is located at $x_r/c = 0.3125$. The motion generated by the pitching mechanism is sinusoidal and defined as: $\alpha(t) = \alpha_m + \alpha_a \times \sin(2\pi f t)$, where $\alpha_m = 0.25°$ is the mean angle of incidence, $\alpha_a = 4°$ is the amplitude and $f = 0.39\,\mathrm{Hz}$ is the frequency and $T = 1/f = 2.55\,\mathrm{s}$ the period of the pitching motion. The reduced frequency of the pitching airfoil motion is $k = \pi f c/U_\infty = 0.09$.

2.2. Flow field measurements

The system used for image recording is a LaVision Minishaker coaxial volumetric velocimetry probe (CVV, [10]) mounted on a Universal Robots UR5 robotic arm, as described in Jux et al. [11]. The flow was seeded with Helium-filled soap bubbles (HFSB, [12]) that were generated by a 200-generator seeding rake, measuring 500 mm × 1000 mm. The seeding rake, producing 6×10^6 bubbles per second in nominal conditions, was placed in the wind tunnel settling chamber; only a subset of the nozzles was functional during the test, which reduced the stream tube size and seeding density, respectively, such that the effectively usable cross-section of the seeded flow region was ca. 200 mm × 200 mm. For the illumination of the HFSB flow tracers, the coaxial illumination of the CVV was not used; instead the illumination was achieved using two LaVision LED-Flashlight 300 units mounted side by side to illuminate a chordwise region of 800 mm length, from 0.5 chord lengths upstream to 0.5 chord lengths downstream of the airfoil. This resulted in a total measurement volume size of about 32 liters. Three different chordwise stations of the CVV probe with respect to the airfoil model were used successively to perform the measurements. The three positions of the CVV with respect to the airfoil are illustrated in figure 2. The distances to the airfoil d_1 and d_2 were about 40 cm, whereas d_3 was about 60 cm. The measurements were performed at mid-span, so that the spanwise component of the flow velocity is expected to be negligible compared to the other two flow components, allowing the flow field to be analyzed in a spanwise-averaged manner. The flow field measurements covered only one side of the airfoil, in view of the symmetry of the pitching airfoil profile. For the non-intrusive load determination, flow field measurements with a phase difference of $\Delta t/T = 0.5$ were combined, so as to reconstruct a flow field measurement that covers both sides of the airfoil.

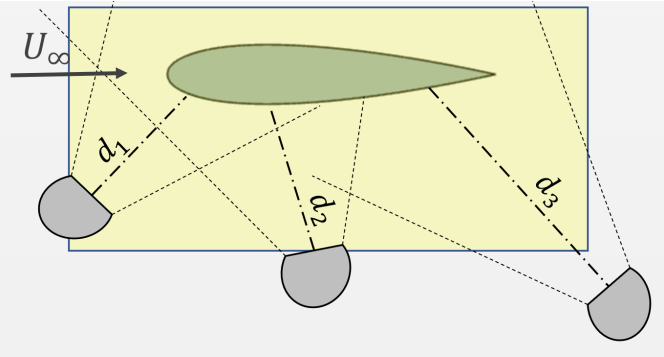

Figure 2. Sketch of the positions of the CVV with respect to the airfoil (not drawn to scale)

Images were acquired in continuous mode at 700 Hz and processed with the LaVision DaVis 10 software. The procedure for obtaining the flow field measurements consists of applying a temporal high-pass filter to the images [13], performing a volume self-calibration [14], generating a non-uniform optical transfer function [15] and then applying the Lagrangian particle tracking algorithm Shake-The-Box [16]. The result from this procedure for the 45 recorded pitching cycles per CVV position is allocated to 100 temporal bins, each spanning 1% of the pitching motion period. Subsequently, the data is ensemble-averaged to a two-dimensional Cartesian grid with 5 mm spacing between adjacent grid points (1.25% of the chord), using an ensemble averaging bin size of $20 \times 20\,\mathrm{mm}^2$ with 75% overlap. The use of a two-dimensional grid in the ensemble averaging produces phase-resolved flow field measurements in a spanwise-averaged sense. The ensemble averaging is performed using a top-hat filtering approach, as described by Agüera et al. [17]. Afterwards, a temporal sliding-average filter with a window size of 5% of the period is applied to each grid point to further reduce the random error in the unsteady flow field data. Four example flow fields for different phase instants are shown in figure 3.

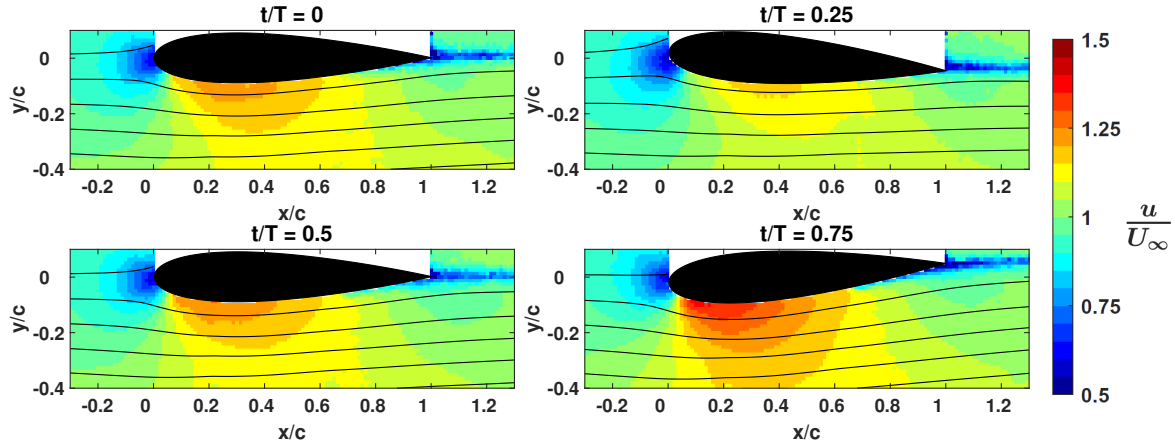

Figure 3. Flow field with streamlines of the pitching airfoil at four phase instants

3. Determination of the unsteady aerodynamic loads

3.1. Method

To calculate the unsteady aerodynamic loads on an airfoil in irrotational flow, one can represent the airfoil by a planar sheet of distributed bound vorticity of strength γ_b along the camber line, following classical thin airfoil theory. In this framework, the unsteady surface pressure difference along the chord $\Delta p(x,t)$ is a function of $\gamma_b(x,t)$ (see [18], chapter 13):

$$\Delta p(x,t) = \rho U_\infty \gamma_b(x,t) + \rho \frac{\partial}{\partial t} \int_0^x \gamma_b(\tilde{x},t) d\tilde{x}. \tag{1}$$

The first term in equation 1 directly relates the instantaneous value of the bound vortex strength distribution $\gamma_b(x,t)$ to the pressure difference via multiplication with a constant factor and is therefore denoted as the quasi-steady pressure difference, expressed as $\Delta p_{qs}(x,t) = \rho U_\infty \gamma_b(x,t)$. The second term accounts for the flow acceleration effects on the surface pressure. The PIV-based load determination begins with the determination of the quasi-steady surface pressure on the surface of the airfoil, which is determined with Bernoulli's equation:

$$C_{p,qs} = \frac{p_{qs} - p_\infty}{q_\infty} = \frac{-q + q_\infty}{q_\infty} = 1 - \frac{V^2}{U_\infty^2}, \tag{2}$$

where V is the velocity magnitude in a region of the flow that can be considered as irrotational and q is the dynamic pressure $q = \frac{1}{2}\rho V^2$. After the quasi-steady surface pressure is determined for one side of the airfoil over the entire pitching motion period, the quasi-steady pressure difference on the airfoil $\Delta C_{p,qs}$ is determined by subtracting measurements of the quasi-steady surface pressure with a phase difference of $\Delta t/T = 0.5$. With this result, the unsteady surface pressure difference including the flow acceleration effects on the pressure can be calculated with equation 1. The first step is to determine the vortex-sheet strength distribution along the chord from the measurement of the quasi-steady pressure difference:

$$\gamma_b(x,t) = \frac{\Delta p_{qs}}{\rho U_\infty} = \frac{\Delta C_{p,qs} \cdot q_\infty}{\rho U_\infty} = \frac{\Delta C_{p,qs} \cdot U_\infty}{2} \tag{3}$$

After calculating $\gamma_b(x,t)$ with equation 3, the result for $\gamma_b(x,t)$ can be used to calculate the unsteady surface pressure difference with equation 1. If the considered angle of attack α remains small, so that $\cos(\alpha) \approx 1$ and the influence of the tangential force on the lift is negligible, the lift coefficient $C_\ell(t)$ and the moment coefficient $C_m(t)$ are obtained by chordwise integration of the pressure difference. In this study, the reference axis for the moment $C_{m,r}$ is the rotation axis of the pitching airfoil.

3.2. Implementation

The quasi-steady surface pressure $C_{p,qs_{surf}}$ cannot be determined accurately from velocity measurements at the surface, in view of measurement errors and viscous effects that affect the near-wall region, and is instead determined using a linear extrapolation of the flow pressure obtained with equation 2 in the vicinity of the pitching airfoil. Similar to the approach of Ragni et al. [6], measurements for a given chordwise location on the airfoil are analyzed along the cross-flow direction of the Cartesian grid. In this study, a zig-zag turbulator strip was placed on the airfoil at $x/c = 0.1$, which promotes the development of a turbulent boundary layer downstream of that chordwise location. Equation 2 is unsuited to determine the pressure inside the turbulent boundary layer, where the effect of viscosity on the flow is not negligible and the flow field is not irrotational. Therefore, the surface pressure is determined in this study using different approaches, depending on the chordwise position, as described in the following and illustrated for five examples in figure 4.

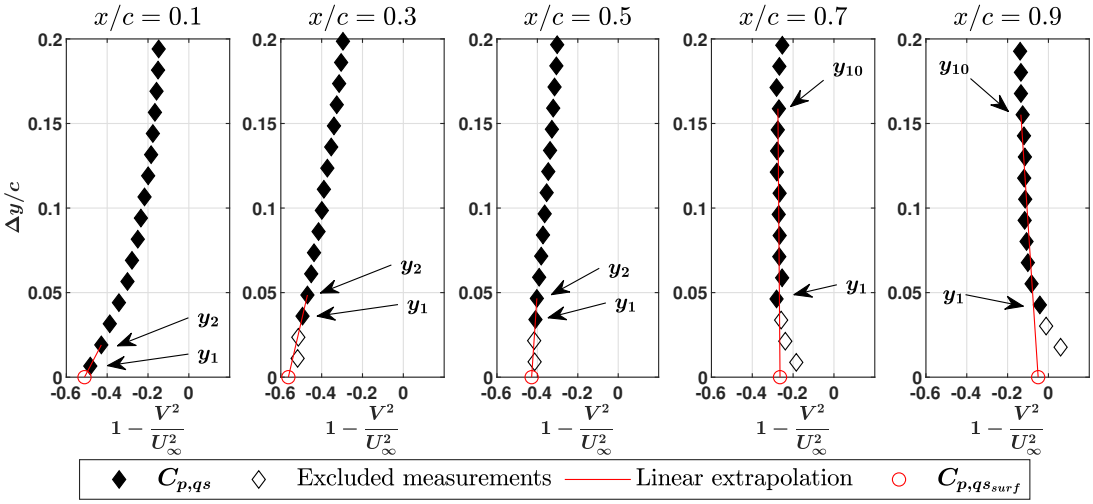

Figure 4. Extrapolation method for the quasi-steady surface pressure at $t/T = 0$

For the chordwise positions with $x/c \leq 0.1$, it is considered that the boundary layer region is laminar and thin, compared to the spatial bin size that is used during the ensemble averaging, so that the flow measurements are not significantly affected by the presence of the boundary layer and equation 2 can be applied close to the airfoil. For $x/c < 0.1$ the quasi-steady surface pressure is therefore determined in three steps:

(i) Application of equation 2 to the flow measurement at the first grid point outside of the airfoil y_1, to determine C_{p,qs_1} at a distance of Δy_1 from the airfoil surface.

(ii) Application of equation 2 to the next following grid point away from the surface in y-direction, y_2 with C_{p,qs_2}, to approximate the pressure gradient $\dfrac{\partial C_{p,qs_1}}{\partial y}$ with a backward finite difference as $\dfrac{\partial C_{p,qs_1}}{\partial y} \approx \dfrac{C_{p,qs_1} - C_{p,qs_2}}{y_1 - y_2}$.

(iii) Extrapolation of the pressure on the surface of the airfoil $C_{p,qs_{surf}}$ from the nearest grid point with $C_{p,qs_{surf}} = C_{p,qs_1} - \dfrac{\partial C_{p,qs_1}}{\partial y} \cdot \Delta y_1$.

For the determination of $C_{p,qs_{surf}}$ downstream of $x/c = 0.1$, it is assumed that the application of equation 2 close to the airfoil surface yields erroneous results due to the presence of a thickened turbulent boundary layer. It is therefore necessary to exclude these data points from the analysis.

The development of the turbulent boundary layer thickness on the airfoil can be roughly estimated using an analytical expression for the turbulent boundary layer thickness on a flat plate with zero pressure gradient $\delta_{BL}(x)$ (see [19], chapter 6):

$$\delta_{BL}(x) \approx 0.16 \frac{x}{Re_x^{1/7}}. \tag{4}$$

Equation 4 is used to exclude the grid points that are likely affected by the presence of the turbulent boundary layer from the surface pressure determination analysis. After that, the determination of the surface pressure follows the same procedure as for $x/c \leq 0.1$. This procedure is illustrated in figure 4 for the chordwise positions where x/c is 0.1, 0.3 and 0.5.

For the flow field measurements where $x/c > 0.65$, more measurement noise is observed. To reduce the sensitivity of the surface pressure result to individual data points, the pressure gradient is not determined from a finite difference in this region, but with a linear regression of multiple data points instead, in this case over 10 data points. This approach also diminishes the modeling errors associated with the application of equation 4 to a region of non-zero pressure gradient, which would affect the measurements at y_1 and y_2. The result of the linear regression is used to extrapolate the surface pressure, as illustrated for $x/c > 0.7$ and $x/c > 0.9$ in figure 4.

4. Results

The chordwise surface pressure difference distribution that is obtained by using the quasi-steady and the unsteady pressure formulations are shown for four phase instants in figure 5. Reference data based on the pressure transducer measurements is shown for comparison. The largest differences between the non-intrusive pressure and the reference appear in the airfoil nose region, for $x/c < 0.1$. It is expected that these larger differences are produced because the spatial resolution of the flow field measurement is insufficient to accurately capture the flow behavior around the nose, which is characterized by relatively large spatial velocity gradients. This problem has also been observed in several previous studies [6,7,8]. Downstream of $x/c = 0.1$, the results are in good agreement with the reference data. The relatively large differences that appear around $x/c = 0.2$ and around $x/c = 0.7$ are considered as measurement artifacts due to the merging of the flow field data from the three different CVV positions. The agreement of the non-intrusive pressure with the reference data is improved compared to the quasi-steady formulation when the unsteady formulation is adopted. The unsteady effects are the largest when the magnitude of the pitch rate is maximal, so around $t/T = 0$ and $t/T = 0.5$. For example, at $t/T = 0.05$, the root mean square (RMS) of the difference to the reference downstream of $x/c = 0.1$ is reduced by about 65% with the unsteady formulation. The aerodynamic loads as determined by a chordwise integration of the pressure difference are shown in figure 6. The behavior of the quasi-steady and unsteady loads over the period is similar, but the inclusion of the unsteady term introduces a phase shift of the signal. The phase shift is negative for the lift and positive for the moment. This can be explained by the fact that the unsteady term affects the load distribution mostly in the region downstream of the reference axis for the pitching moment computation that is located at $x_r/c = 0.3125$, as it is observed in figure 5. This means that an increase in lift due to the inclusion of the unsteady term corresponds to a nose-down, therefore negative, pitching moment and vice-versa, hence the opposing phase shift. For the lift and the moment, including the unsteady term produces a significant improvement in the agreement with the reference data in comparison to the quasi-steady loads. For the lift coefficient C_ℓ, including the unsteady term results in a phase shift of $\Delta t/T = -2.2\%$, and the RMS of the difference to the reference is reduced by 33%. For the moment $C_{m,r}$, the phase difference between the quasi-steady result and the unsteady result is $\Delta t/T = 5.2\%$, and the RMS of the difference to the reference is 54% lower for the unsteady result.

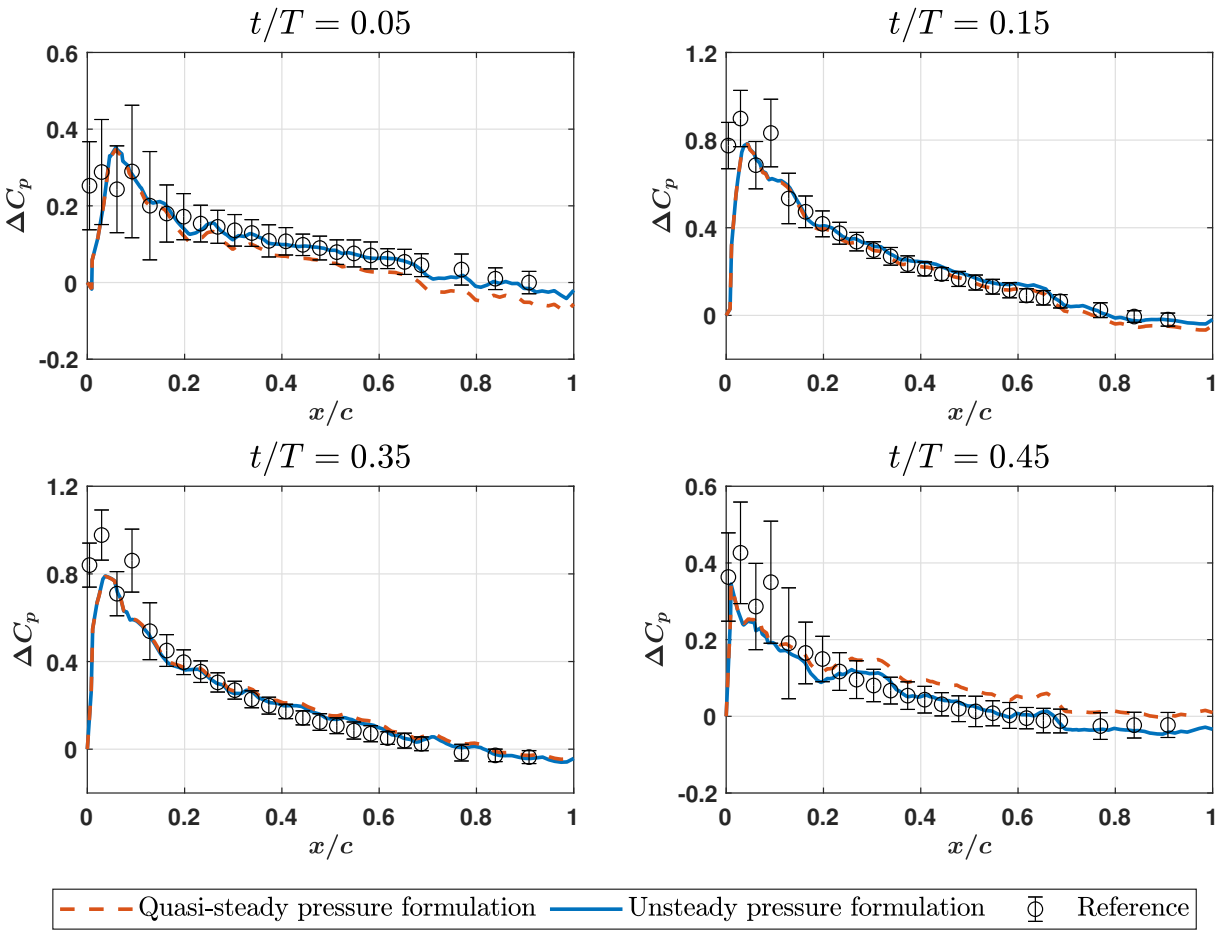

Figure 5. Comparison of the PIV-based surface pressure difference with the reference data

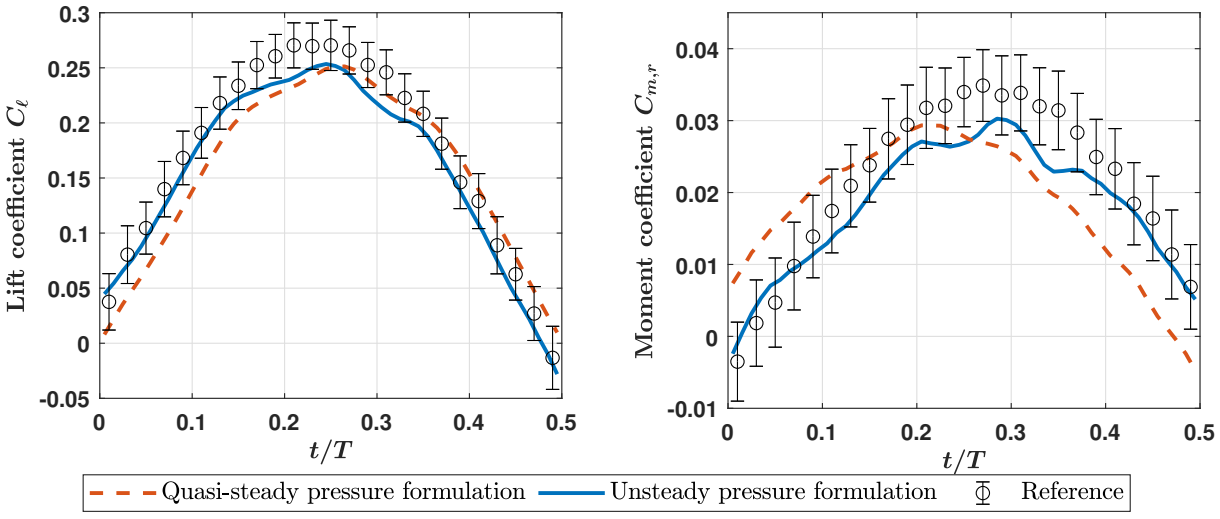

Figure 6. Comparison of the PIV-based aerodynamic load coefficients with the reference data

5. Conclusion

The unsteady aerodynamic loads in terms of the surface pressure difference, the lift and the pitching moment on a pitching airfoil were determined non-intrusively from measurements of the flow velocity obtained with a robotic PIV system. The unsteady surface pressure was determined by first calculating the quasi-steady flow pressure in the vicinity of the airfoil with Bernoulli's equation. Subsequently, relations from unsteady potential flow and thin airfoil theory were used to account for the unsteady aerodynamic effects. It was observed that the difference between the results and the reference data from the pressure transducers installed in the airfoil is decreased by more than 50% when the unsteady pressure formulation is used, compared to results from a quasi-steady approach using only Bernoulli's equation. The largest remaining discrepancies with the reference occur in the airfoil nose region, where the spatial resolution of the PIV measurement is insufficient to accurately capture the flow behavior, which is characterized by relatively large spatial gradients.

The lift and the pitching moment that act on the airfoil were obtained by integrating the determined surface pressure difference. The consideration of the unsteady effects on the loads is highly effective for increasing the agreement with the reference data, as expected from the analysis of the pressure difference. The improvements originate primarily from a shift of the quasi-steady results in phase, that occurs when the unsteady effects are included.

Although the analysis of the pitching airfoil in this study was performed in a two-dimensional sense, the measurement data is obtained in three-dimensional space, hence a wider range of potential applications exists. However, considering that the aerodynamic loads determination methods in this study were derived based on the assumption of unsteady potential flow, further research is necessary to assess the performance and consider possible adaptations for the application of these methods in flow situations where the viscous effects are more dominant, such as in the case of separated flow over the airfoil.

Acknowledgments

This work has been carried out in the context of the HOMER (Holistic Optical Metrology for Aero-Elastic Research) project that has received funding from the European Union's Horizon 2020 research and innovation programme under grant agreement No 769237.

References

[1] Van Oudheusden B W 2013 *Meas. Sci. Technol.* **24** 032001
[2] Kurtulus D, Scarano F and David L 2007 *Exp. Fluids* **42**(2) 185-96
[3] Villegas A and Diez F J 2014 *Renew. Energy* **63** 181-93
[4] De Kat R and van Oudheusden B W 2012 *Exp. Fluids* **52** 1089–106
[5] Gharali K and Johnson D A 2014 *Exp. Fluids* **55** 1803
[6] Ragni D, Ashok A, van Oudheusden B W and Scarano F 2009 *Meas. Sci. Technol.* **20** 074005
[7] Tagliabue A, Scharnowski S and Kähler C J 2016 *J. Vis. (Tokyo)* **20**(3) 581-90
[8] Jux C, Sciacchitano A and Scarano F 2020 *Meas. Sci. Technol.* **20** 074005
[9] Raiola M, Discetti S, Ianiro A, Samara F, Avallone F and Ragni D 2018 *AIAA J.* **56**(4) 1388-401
[10] Schneiders J F G, Scarano F, Jux C and Sciacchitano A 2018 *Meas. Sci. Technol.* **29** 065201
[11] Jux C, Sciacchitano A, Schneiders J F G and Scarano F 2018 *Exp. Fluids* **59** 74
[12] Scarano F, Ghaemi S, Caridi G C A, Bosbach J, Dierksheide U and Sciacchitano A 2015 *Exp. Fluids* **56** 42
[13] Sciacchitano A and Scarano F 2014 *Meas. Sci. Technol.* **25** 084009
[14] Wieneke, B 2018 *Meas. Sci. Technol.* **29** 084002
[15] Schanz D, Gesemann S, Schröder A, Wieneke B and Novara M 2013 *Meas. Sci. Technol.* **24** 024009
[16] Schanz D, Gesemann S and Schröder A 2016 *Exp. Fluids* **57** 70
[17] Agüera N, Cafiero G, Astarita T and Discetti S 2016 *Meas. Sci. Technol.* **27** 124011
[18] Katz J and Plotkin A 2001 *Low speed aerodynamics* (Cambridge University Press)
[19] White F M 2006 *Viscous fluid flow* (McGraw-Hill)